Magnetic cellular automata and the formation of glassy and magnetic structures from a chain of magnetic particles

D. M. Forrester,[1] K. E. Kürten,[1,2] and F. V. Kusmartsev[1,3]
[1]*Department of Physics, Loughborough University, Loughborough LE11 3TU, United Kingdom*
[2]*Institut für Experimentalphysik, Universität Wien, Austria*
[3]*L. D. Landau Institute for Theoretical Physics, Moscow, Russia*
(Received 24 April 2006; revised manuscript received 12 October 2006; published 11 January 2007)

We show that magnetic materials made of chains of small magnetic particles display many unusual properties. This is associated mainly with a variety of stable different magnetic structures which can arise there. In particular, there arises a magnetic glass, which may be characterized by a whole set of hysteresis loops and by a large variety of Barkhausen jumps arising in the returned branches of the hysteresis loops. We consider in detail a simple example of such a system—a chain of magnetic nanoparticles. To describe such a single chain first we use numerical micromagnetic simulations. On the basis of these simulations, with the use of a perturbation theory, we derive an analytical model which is an anisotropic Heisenberg model. This is a Heisenberg model with an additional anisotropy term arising due to the shape of the particles. Such a term also arises naturally in some classical magnetic materials such as Mn_2Ni chains. We describe all possible stable states of the system as well as transitions between the states induced by magnetic field. Each of these transitions is arising *a la* the spin flop transition. It may be displayed and detected in experiments as a Barkhausen jump in a hysteresis loop. The series of described spin flop transitions will lead to the formation of different types of returned branches in hysteresis loops. We present exact analytical and numerical results describing the energy spectrum and the magnetization of such systems. The results may be used in the design of nanomaterials as well as for magnetic random access memory and magnetic quantum cellular automata elements.

DOI: 10.1103/PhysRevB.75.014416 PACS number(s): 75.75.+a, 05.50.+q, 75.10.Hk, 75.60.Ch

I. INTRODUCTION

The nanocomposite materials consisting of small magnetic nanoparticles are novel types of materials which display many useful features unusual for conventional magnetic materials.[1] Their magnetic responses depend on the particle sizes, particle shapes, as well on as the distance between particles.[2,3] In many situations magnetic particles may have at least two well-defined magnetic states. Therefore such nanocomposite materials could serve as building blocks for new nanoscale magnetoelectronic devices and data storage media. Indeed, recently, Zhu *et al.* have produced a film made of small magnetic nanodots. Such a film may operate as a powerful magnetic storage device on the scale of billionths of a meter.[4] On the other side, Cowburn and Welland proposed the use of a chain of magnetic nanoparticles deposited on a nonmagnetic substrate as a room temperature magnetic quantum cellular automata (MQCA).[5,6] Such automata, made of magnetic nanodots, are capable of data handling. The silicon microchip, the single electron transistor (SET) may generate the next revolution in data processing and storage. Arrangements of SETs have recently shown their ability to perform logic operations. They were called quantum cellular automata (QCA) because they use quantum mechanical tunneling of charge between quantum dots to change a logic state. Currently, the electronic QCA will only work at milliKelvin temperatures. Therefore the attention is now focused on magnetic QCAs instead, which can operate at room temperatures. The MQCA networks are typically built up of magnetic dots that are 110 nm across and 10 nm thick with a pitch of 135 nm and they are made from a common magnetic alloy on a silicon substrate. It was found that such a MQCA was able to work even at room temperature.[5,6] At low temperatures the ferromagnetic exchange interaction between spins in a single dot is forming a single giant classical spin. Magnetic interactions between nearest neighbors along the chain of dots allow the propagation of information, but also force the magnetization to point along one of the directions of the main anisotropy of the chain, producing a natural binary logic system. The direction of the dot's magnetization vector is supposed to indicate a logic state. The logic state can be set by applying a single magnetic pulse at the first input dot. An oscillating microwave magnetic field can then reverse the magnetic state of the chain of dots, changing the logic state, as a magnetic soliton propagates along the chain. This soliton or better to say the kink, like a domain wall in a bulk material, separates regions of left and right magnetization. Normally in homogeneous media solitons propagate without loss. However, small fluctuations in the shape of the dots are forming inhomogeneities and will cause the soliton to dissipate energy as it propagates. We believe that the magnetic QCA "has enormous potential" to meet the requirements of digital processing of the future.[5] Cowburn *et al.* have realized various linear chains where all particles were ferromagnetically or antiferromagnetically coupled. There magnetic moments were oriented along or perpendicular to the chain. The orientation of the magnetic moments has been controlled by a particle, deposited at the beginning of the chain, which was different (larger or more elongated) than the other particles. Normally this first particle had a distinguished ellipsoidal or cigar shape. It was shown[5] that by using a slightly biased, pulsed magnetic field that the magnetic moments associated with these individual particles are flipped coherently, in a fashion comparable to a "domino"

 ©2007 The American Physical Society

effect. In the magnetic automata the value +1 corresponds to one spin orientation of the single particle, while the value −1 corresponds to the opposite spin orientation. Moreover, it was demonstrated that it is possible to form logic chains from such particles.[8,9]

Recently a temperature dependence of the magnetization reversal of an analogous system such as a single-chain magnet has been studied.[10] This single-chain magnet is a heterometallic chain of Mn^{III} and Ni^{II} metal ions called an Mn_2Ni chain (see Ref. 10 for details). Such a chain consists of ferromagnetically coupled $S=3[Mn^{III}-Ni^{II}-Mn^{III}]$ units and is naturally described by an anisotropic Heisenberg model. It was found that the shape of the hysteresis loop and the nucleation energy for a domain wall creation depend on the magnetic field and its sweep rate as well as on the temperature T. At very low temperatures the reversal of the magnetization is induced by a quantum nucleation of a domain wall that propagates due to the applied field.

We have shown that all these systems display a variety of unusual features not present in bulk magnetic systems associated with the formation of the domain structures. In the framework of the anisotropic Heisenberg model we describe analytically and numerically a formation of an arbitrary number of domain walls. Obviously if all these spins are originally ferromagnetically oriented, then the switch or a spin flip of one element corresponds to a creation of two domain walls (domain and antidomain walls). In particular, we show that all relevant physical quantities such as the values of magnetic moments of the particles, the energy spectrum, coercive forces, and hysteresis loops may display fractal structures, similar to those found for the Ising chain.[11] The formation of fractal structures is very subtle. It is mostly related to a competition between anisotropy and interparticle interactions of the associated semiclassical magnetic moments forming the chains.

II. NUMERICAL MODELING

First of all we would like to make micromagnetic simulations to investigate real monodomain magnetic particles, the distribution of magnetic fields around these particles, and the characteristic energies of their interaction. Having this in mind we consider a few magnetic particles made from Fe deposited on Si substrate, on the X-Y plane, see Fig. 1. The Si substrate is denoted by a gray color while the Fe particle by a darker color. Let us assume that all these particles are disk-shaped ellipses, see Fig. 1. Such a setup was used in experiments.[5,6,9] The size of the particles is so small that they can be considered as having a single domain. Their magnetization M is polarized along the main axes of their anisotropy which is oriented along the main axis of the ellipses, let us say along the Y axes. We would like to investigate the distribution of magnetic fields associated with these particles as well as how the magnetization of these particles will be changed when a magnetic field is applied. Then we apply a magnetic field in the X-Y plane oriented along the (1,1,0) direction. As in past experiments (Refs. 5, 6, and 9) each particle is a disk which has a geometrically elliptical shape. Along the main axis of the ellipse the length is 135 nm, the width is equal to 70 nm, and height is 30 nm. The separation between the centers of each pair of particles is taken to be 135 nm in the x-direction of the model, see Fig. 1. The distribution of the vector potential $A(r)$ and stray magnetic field in a space within and between the particles may be found from the numerical solution of the following system equations.

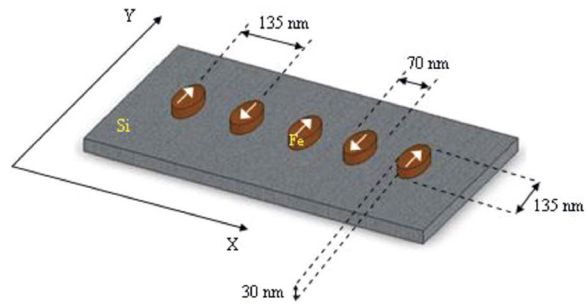

FIG. 1. (Color online) Five elliptically shaped magnetic particles in a linear chain. The particles are made from iron and are deposited upon a silicon substrate. As in past experiments (Refs. 5, 6, and 9) each particle has an elliptical geometry. Along the main axis of the ellipse the length is 135 nm, the width is equal to 70 nm, and height is 30 nm. The separation between the centers of each pair of particles in the x-direction is taken to be 135 nm.

$$\nabla \times [\mu_0^{-1}\mu_r^{-1}(\nabla \times A - M)] = 0, \tag{1}$$

where A is a vector potential, M is a magnetization, μ_0 is the permeability of free space equal to $4\pi\times 10^{-7}\ N/A^2$, and μ_r is the relative permeability which is material dependent (we have taken it to be 4000 for iron). On the boundary of each particle the tangential component of magnetic field is a continuous function that results in the following boundary conditions

$$\nabla \times A \times \mathbf{n}|_{\partial\Omega} = H \times \mathbf{n}, \tag{2}$$

where $\mathbf{n}$ is the normal vector defined on the boundary $\partial\Omega$ associated with all particles. Here H is the value of the applied field, while the value $B(r)=\nabla\times A(r)$ is the field resulting from the external field and the magnetization of particles.

The magnetic field distributions associated with these particles of nanoscale proportions are investigated numerically. This is done with the use of finite element methods in FEMLAB. First we solve the equations (1) with the use of the boundary conditions, Eq. (2). Then we calculate the total energy and the total magnetization of the system as a function of magnetic field strength H. The models mesh consists of 12,425 bulk elements.

Next, to estimate the magnetic energy we use the following equation:

$$E_{mag} = \int_{space} \frac{B^2}{8\pi} dV, \tag{3}$$

where the integration is taken over the space around these particles. We consider an example of five particles made from Fe and arranged in a linear array as depicted in Fig. 1.

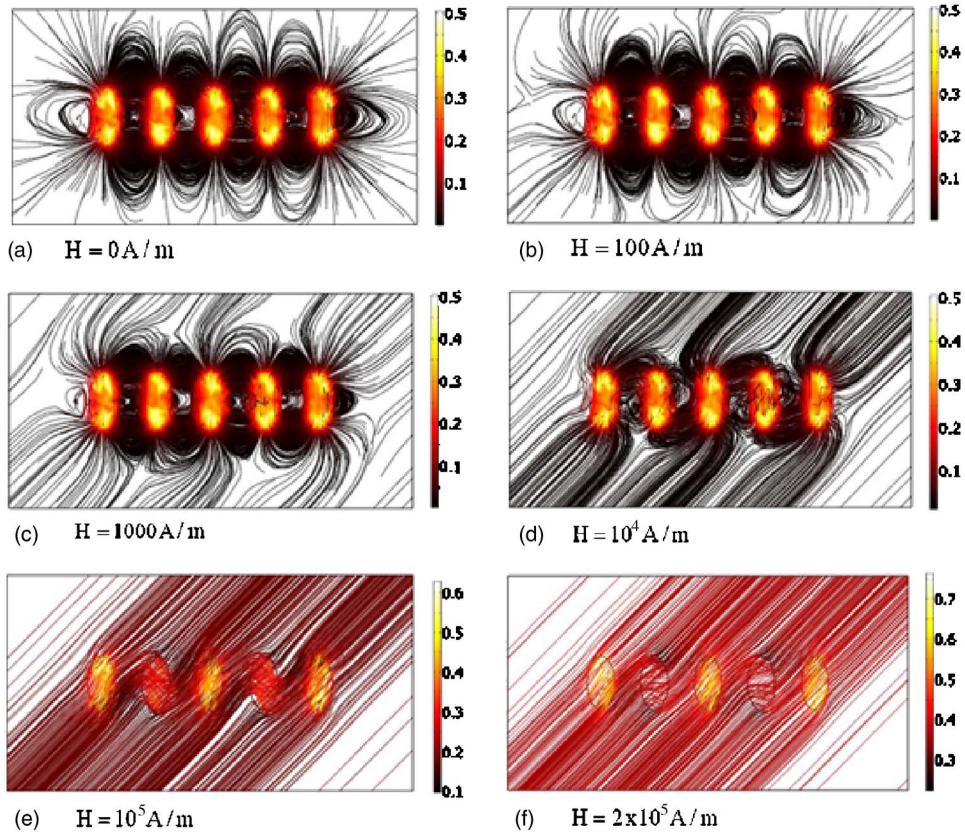

FIG. 2. (Color online). The field lines of magnetic flux density calculated at six values of the magnetic field strength H equal to: (a) zero field, (b) 100 A/m, (c) 1000 A/m, (d) 10^4 A/m, (e) 10^5 A/m (f) 2×10^5 A/m. At $H=0$ the magnetic flux density is at its highest level deep inside the particles, illustrated by ellipses. As we step out from the core of the particles this high flux density begins to scale down, as can be seen around their elliptical perimeters, until we reach the flux density in the surroundings. The highest value of magnetic flux density is around 0.5 T in the particles, dropping to a minimum marginally larger than zero in the outer environment. As the magnetic field strength is ramped upwards these values remain fairly consistent, up to much higher field levels, except that we see an aligning of the flux density with the field strengths direction. As the field continues to elevate the second and fourth particles, originally magnetized against the field, experience a slight drop in their flux densities, whereas their neighbors begin to compensate by taking higher ones. In the final diagram in the depicted sequence, at 2×10^5 A/m, the outer particles and the central one find their highest magnetic flux densities while the others have their lowest. Finally, the system has undergone a complete ferromagnetic polarization.

Without an external magnetic field each particle may have two stable states when the magnetization of this particle is oriented along the Y-direction. From first glance one may notice that these particles have a dipole-dipole type of interparticle interaction. In the absence of an external magnetic field different locally stable states correspond to the different configurations of magnetization of these particles. Here the total number of configurations will be $2^5=32$. The low energy state should correspond to antiferromagnetic ordering of these particles. The excited states will correspond to situations when one or a few of these particles will flip its magnetic moment.

Now let us apply an external magnetic field and calculate the magnetic flux density by solving the equations (1) with the boundary conditions, Eq. (2). The result of these calculations is presented in Fig. 2 where the particles are illustrated by ellipses. There we present the distribution of the magnetic flux density calculated at six different values of magnetic field applied in the (1,1,0) direction. At zero field the particles are in a ground state, i.e., in an antiferromagnetic configuration. We choose the elliptical shape of the nanoparticles disks to ensure that shape anisotropy dictates. The magnetizations find preference in aligning themselves along the long axes of the particles as a result. The stray field surrounding the ellipses indicates clearly the antiferromagnetic interaction between the particles. When the magnetic field is applied at an angle of 45°, in the X-Y plane, one may notice how the stray field is deformed. The individual particles have uniform magnetizations. A simple interpretation may be done with the use of imaginable "magnetic" charges.[12] So even with no external magnetic field the elliptical shape provides for surface "magnetic" charges to appear at the extremities of the longitudinal axes. Consequentially these charges are a source of a magnetic field. As the magnetic field strength increases the magnetic flux density associated with these particles becomes more and more polarized along the external field direction of application. In Fig. 2 we present six images of the magnetic flux distribution. In the first image there is no external field. It shows perfect antiferromagnetic ordering. As the magnetic field equal to 100 A/m is applied the magnetic configuration is still the same. However, at the next magnetic field equal to

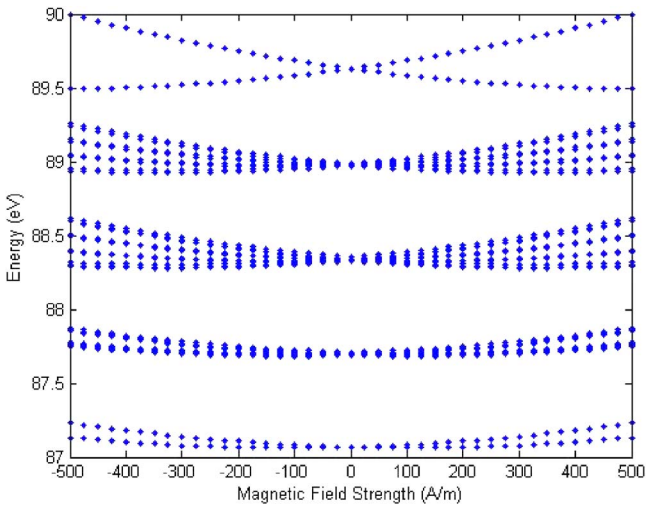

FIG. 3. (Color online) The magnetic energy of the system of particles E as a function of external magnetic field strength H. The bands directly correspond to the different number of antiphase domain boundaries (or domain walls in antiferromagnetic ordering) that arise for different magnetization orientations in the system as a whole.

1000 A/m one sees that the antiferrimagnetic ordering is weakened, although it still exists. At the next magnetic field equal to 10^4 A/m the particles are very weakly antiferromagnetically coupled. Finally at the field 10^5 A/m all magnetic moments of particles are flipped and they are in the ferromagnetic state. The forthcoming increase of magnetic field sees the particles remain in the ferromagnetic state.

Now let us estimate the energy of these particles for different (32) configurations of their magnetic moments. This energy as a function of external magnetic field is presented in Fig. 3. At zero field one may notice five equidistant energy levels. These levels are transformed into the bands if we also take into account nonzero field. The lowest two energy branches correspond to the antiferromagnetic ordering whereas the top two relate to the ferromagnetic ordering of the magnetic moments of these particles. The first "band" associated with the first excited group of branches is representative of one antiphase domain boundary in the antiferromagnetic ground state ordering. The second excited group of branches (the second band) corresponds to two antiphase domain boundaries in the antiferromagnetic ordering. The third excited group of energy branches are in turn associated with three antiphase domain boundaries in the antiferromagnetic ordering. Finally, four antiphase domain boundaries in the antiferromagnetic ordering correspond to the ferromagnetic ordering. For each of these 32 configurations the energy of the system is found to respond to field strength as shown in Fig. 3. All the particles interact with one another but from the analysis of the energy spectrum we may conclude that the strongest is the interaction between the nearest neighbors. This constant may be estimated from the obtained energy of the antiphase domain boundary.

Now let us estimate the energy separation between the energy bands calculated at zero field. From Fig. 3 we see that it is equal to 0.6 eV. It is now necessary to remember that in the magnetic automata the value $S_i=+1$ corresponds to one spin orientation of the single ith particle, while the value $S_i=-1$ corresponds to the opposite spin orientation. Such a choice of spins is convenient for the construction of different magnetic logic.[8,9] Therefore the interaction between two neighboring particles in such magnetic cellular automata will be equal to $J_0 S_i S_{i+1}$. Thus when there is no externally applied magnetic field, we have defined J_0 as the nearest neighbor coupling constant of the spin one particles forming magnetic cellular automata. If the ground states of such automata are of an antiferromagnetic type, as in the considered example, i.e., $J_0>0$ then the cost of one antiphase domain boundary will be equal to $2J_0$. Then, from the energy spectrum presented in Fig. 3 we obtain that the nearest neighbor coupling constant J_0 is around 0.3 eV. From the analysis of the energy spectrum presented in Fig. 3 we may obtain the coupling constant between next nearest neighbors and all other constants of interaction between all particles. However, they are significantly smaller than the constant of nearest neighbor interaction J_0. The proximity of the particles generates the characteristic that there is not simply a dipole-dipole relationship and the interaction has a much more complicated form, i.e., other multipoles should exist. On the other hand, our micromagnetic investigation indicates that the interaction between nearest neighbors is the most important. This allows us to derive a simple model which may have an analytic solution for any number of particles. This model will be derived in the next section and is called an anisotropic Heisenberg Hamiltonian.

III. PERTURBATION THEORY AND ANALYTICAL MODEL

Let us consider a linear chain made of small magnetic particles. To describe this very complicated system in a straightforward way is to use micromagnetic simulations in a manner as was used for many complicated systems. This is done by taking into account all existing interactions such as an interaction between quantum magnetic moments inside the particles, the surface effects, and the interaction between the particles. Such numerical simulations have always been useful ever since the invention of the computer. Indeed there recently appeared many such useful simulations, like the one made above. However, one may obtain a more extensive picture of the behavior of the system in an even more simple and elegant way if we notice that there is a hierarchy of existing interactions. The strongest interaction is the exchange ferromagnetic interaction J_{inside} between quantum magnetic moments inside single particles. Due to this interaction all magnetic moments inside the particle are oriented in the same direction forming a single large classical moment. For small particles the surface effects form the second level of this hierarchy of interactions. The surface and the shape of the particle give rise to the shape anisotropy of a single particle described by a large shape anisotropy constant K. Obviously the value of K is much smaller than J_{inside}. Due to this anisotropy the total magnetic moment of a single particle may have some preferred directions. For example, for elongated particles it will be directed along the main axes of

symmetry. Finally, the third level of the hierarchy is formed by an interaction between particles. The type of this interaction depends mostly on their surroundings. If the surrounding material is a metal then it will be an RKKY interaction as the dominant one, otherwise only dipole-dipole and other multipole interactions remain. The latter depends on the orientation of the particles and obviously is significantly weaker than the other two types of interactions described above, such as the exchange interaction within a particle and the anisotropy constants. This hierarchy of interactions allows the derivation of the model describing the system of magnetic nanoparticles by the anisotropic Heisenberg Hamiltonian. With the use of the perturbation theory, making an expansion with the parameter $K/J_{inside} \ll 1$, we reduce the number of relevant parameters and finally the chain of magnetic particles is described by an anisotropic Heisenberg Hamiltonian. The zero approximation gives that small particles are single domain objects and therefore each particle may be characterized by a large magnetic moment. The first approximation gives the anisotropic Heisenberg model. Thus the model has been derived with the use of the perturbation theory, which is justified on the basis of a hierarchy of existing interactions. This model describes a realistic system consisting of a chain of magnetic particles on an equal footing with micromagnetic simulations.

Such linear chain systems have already been produced from small ferromagnetic particles made, for example, of Fe (see also, Refs. 5, 6, and 13). If all spins within a single particle are ferromagnetically ordered, then each particle may be considered as a single classical spin $\vec{S}$. Then the chain of magnetic particles having a disk or elliptic shape can be described by a model of interacting classical spins, that is by the anisotropic Heisenberg Hamiltonian:

$$E = -\sum_{\langle i,j \rangle} J_{ij}\vec{S}_i\vec{S}_j - g\mu_B\mu_0\sum_i \vec{H}\vec{S}_i + \sum_{i\alpha} K_\alpha S_{i\alpha}^2. \tag{4}$$

Here we assume that magnetic moments associated with individual magnetic disks are interacting via dipole-dipole interaction characterized by the constants J_{ij}, which also depend on the orientation of the appropriate magnetic moments $\vec{S}_i$ and $\vec{S}_j$, where $\vec{S}=(S_x,S_y,S_z)$; and magnetic field $\vec{H}=(H_x,H_y,H_z)$. Each magnetic disk is characterized by anisotropy constants K_α, where $\alpha=x,y,z$. We also assume that the disks are located in the (x,y) plane of a substrate, so that the z-axis is perpendicular to the disk plane. The value of the configurational anisotropy constant K_z associated with the disk shape is the largest. It is much larger than the constants of in plane anisotropy, K_x and K_y, i.e., $K_z/K_x \gg 1$ and $K_z/K_y \gg 1$. We also assume that $K_x \gg K_y$, that is the particles have the shape of ellipses (see Fig. 1).

Within each particle all magnetic moments are ferromagnetically aligned but with an orientation differing from particle to particle the system can be modeled as a collection of N elementary classical magnetic moments, which can be described by a classical Heisenberg Hamiltonian. For the disk shaped particle the value of $\vec{S}_i=[s\cos(x_i), s\sin(x_i), 0]$, where x_i is an angle describing an orientation of magnetic moments within the plane. Below we use notations and units where $H=g\mu_B\mu_0 hs$ with $h=\sqrt{H_x^2+H_y^2+H_z^2}$, $K=2K_y s^2$, and we only take into account the nearest neighbor interaction $J_{i,i+1}s^2 = J\delta_{i,i+1}$. Then, the total energy of such a spin chain is given by the N-particle Hamiltonian

$$E = \sum_{i=1}^{N}\left(-J\cos(x_i - x_{i-1}) - H\cos(x_i - \beta) + \frac{K}{2}\sin^2(x_i)\right), \tag{5}$$

where, for simplicity, periodic boundary conditions are imposed. Here, the variables x_i specify the angles between the magnetizations of the individual particles and the axis of symmetry of the individual single particles. Depending on the orientation of the magnetic moments the dipole-dipole coupling constant J may take positive or negative values. Suppose that all particles having the shape of ellipses are oriented perpendicular to the chain as in Fig. 1. Then due to the shape anisotropy the leading term of the dipole-dipole type of interaction between particles associated with the value of J is antiferromagnetic, i.e., $J<0$. The Zeeman energy, defined by the strength of an external magnetic field H, favors the alignment of the moments along the field direction. The quantity β defines the angle between the reference symmetry axis of individual particles and the external magnetic field, while the quantity K specifies the strength of the particle anisotropy. Besides the energy, another important macroscopic quantity of interest is the total magnetization m taken along the direction of the magnetic field. Defined as

$$m = \frac{1}{N}\sum_{i=1}^{N}\cos(x_i - \beta), \tag{6}$$

this quantity specifies an average over the magnetic moment directions of the individual magnetic particles with respect to the magnetic field orientation. Locally stable equilibrium configurations obey the set of N nonlinear coupled equations

$$J[\sin(x_i - x_{i-1}) + \sin(x_i - x_{i+1})] + H\sin(x_i - \beta) + \frac{K}{2}\sin(2x_i) = 0. \tag{7}$$

As noted before magnetic submicron particles are typically characterized by a high value of the anisotropy constant K associated with their shapes. It is normally much larger than the absolute value of the interparticle spin-spin interaction J. The large number of experimentally possible observed locally stable spatial structures in the magnetic chains is a simple consequence of the variety of possible magnetic domain structures. By the transformation into two mappings these equations at zero field, $H=0$, have been studied in Ref. 14. The existence of a rich diversity of domain wall solutions related in a bifurcation scenario was proven there. Magnetic domains and solitons result from the balance of several competing energy contributions, where the system tries to compromise between all the competing forces. When the three control parameters H, K, and β vary, the energy balance is changed such that a rearrangement of the domain structure can take place.

IV. THE ENERGY SPECTRUM AS A FUNCTION OF THE MAGNETIC FIELD

In order to get some first insight into the structure of the energy spectrum let us first consider the system at zero magnetic field $H=0$, where Eq. (4) reduces to

$$J[\sin(x_i - x_{i-1}) + \sin(x_i - x_{i+1})] + \frac{K}{2}\sin(2x_i) = 0,$$

$$i = 1,2,\ldots,N. \tag{8}$$

For sufficiently large values of K this set of equations has exactly 2^N distinct locally stable solutions consisting of "binary" vectors $\mathbf{x}^* = (x_1^*, x_2^*, \ldots, x_N^*)$ with $x_i^* \in \{0, \pi\}$. These solutions are associated with spin up and spin down orientations of magnetic moments of individual particles.

Accordingly, for $\frac{H}{K} \ll 1$, in zero order approximation, the energy E_m associated with local minima takes the simple form

$$E_m = -J\sum_{i=1}^{N} \cos(x_i^*)\cos(x_{i-1}^*) - H\cos(\beta)\sum_{i=1}^{N} \cos(x_i^*), \tag{9}$$

with $x_i^*\{0, \pi\}$. Note that the first sum is related to the number of domain walls N_d via

$$\sum_{i=1}^{N} \cos(x_i^*)\cos(x_{i-1}^*) = N - 2N_d, \tag{10}$$

while the second sum is related to the zero order magnetization m_0 via

$$\sum_{i=1}^{N} \cos(x_i^*) = m_0. \tag{11}$$

In contrast to the total magnetization m, defined in Eq. (6), the quantity m_0 is measured with respect to the easy axis and is not normalized per particle as m. Due to our periodic boundary conditions the number of domain walls N_d is an even number satisfying the inequality $0 \le N_d \le N-1$ for N odd, and $0 \le N_d \le N$ for N even. The number of distinct values of the zero order magnetizations m_0 depends linearly on the number of domain walls N_d. For the two homogeneous configurations with all spins up ($x_i=0$) and all spins down ($x_i=\pi$), where N_d is zero, m_0 can only take the two values, N and $-N$, respectively. For the other antiferromagnetic limit, $N_d=N-1$ for N odd as well as $N_d=N$ for N even. Here we have the maximum number of domain walls associated with the antiferromagnetic order and the value $m_0=0$ for N even, and there are two values $m_0=\pm 1$ for N odd. For all other domain wall configurations with $N_d \neq 0$ it is easy to verify that the number of distinct possible values for m_0 is $N-N_d+1$ for N odd and $N-N_d+2$ for N even.

Eventually, for fixed N_d and m_0, the zero order energy E_m is a linear function of the magnetic field H and can be written in the more compact form

$$E_m = -J(N - 2N_d) - m_0\cos(\beta)H. \tag{12}$$

levels is $N^2/4+2$ for N even and $(N^2-1)/4+1$ for N odd. In general terms, each energy level of the system corresponds to a configuration associated with a local minimum, a different number of domain walls N_d and different value of the total magnetization of the chain $m_0=N_+-N_-$, where N_+ is the number of spin-up particles while N_- is the number of spin-down particles. So the magnetization m_0 may be viewed as the total magnetic moment of the chain. It is an integer number being even for N even and odd for N odd.

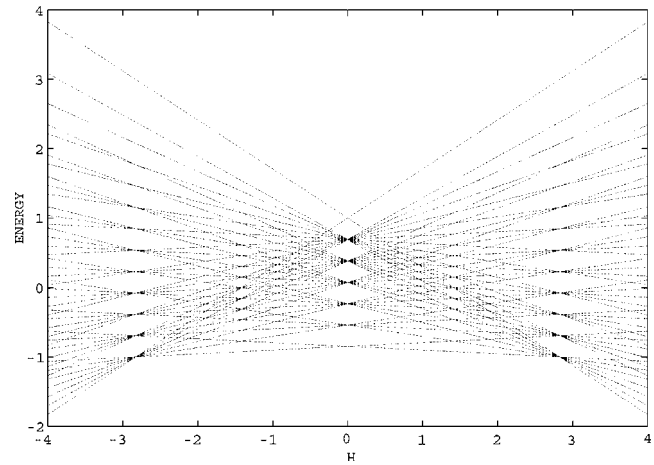

FIG. 4. Normalized linear energy spectrum of local minima E as a function of H for the value $\beta=\frac{\pi}{4}$ and $K=5.5J$. The number of magnetic particles in the chain is equal to $N=13$. The energy associated with a vertical axes is measured in the units of the interparticle interaction constant $J=J_d s^2$, where J_d is a constant of the dipole-dipole interaction and s is the total spin momentum of an individual particle. The magnetic field H is measured in the units of J. The real value of magnetic field may be obtained from the value of H by the multiplication of $J/g\mu_B\mu_0 s$, where g is the Lande splitting factor and μ_B is the Bohr magneton.

$$-(N - N_d) < m_0 < N - N_d. \tag{13}$$

The corresponding linear energy spectrum, as a function of the external magnetic field H, for $N=13$ is depicted in Fig. 4. For $H=0$ we find exactly seven distinct energy values. The energy of the lowest minimum corresponds to the configuration with 12 domain walls, followed by the configurations with 10, 8, 6, 4, and 2 domain walls, while the highest energy is occupied by the two homogeneous configurations with no domain walls at all.

For $H \neq 0$ the number of possible distinct magnetizations m_0 comes into play such that according to the number of domain walls the seven energy levels split into 2, 4, 6, 8, 10, 12, and 2 sublevels, respectively. The two ferromagnetic energy configurations without domain walls ($N_d=0$) represent an exception from this scheme. From Eqs. (9) and (10) one may see that the chain behaves as a giant quantum particle, where the moment is quantized in units of two with the exception that the maximum momentum $m_{0_{max}} = \pm N$ is not quantized and takes only these two values.

Note that the linear energy spectrum does not give us any insight into the local stability or existence of these energy levels for arbitrary values of H. Therefore, to find the critical stabilities for the individual local minima we have to solve the full set of coupled, nonlinear relaxation equations

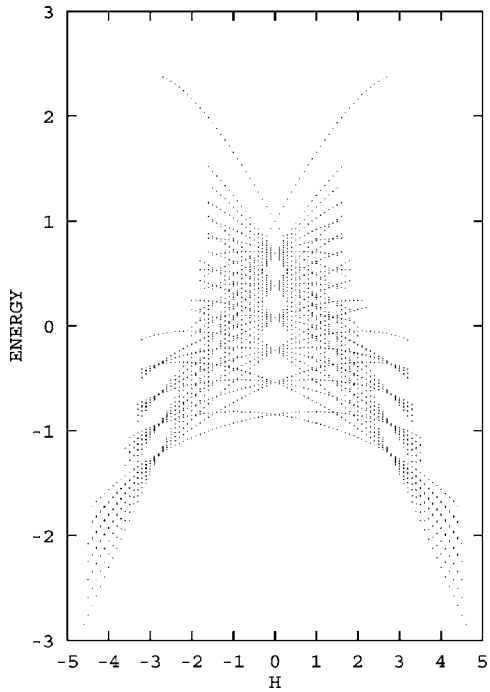

FIG. 5. The spectrum of energies E associated with local minima as a function of magnetic field H for the value $\beta=\frac{\pi}{4}$ and $K=5.5J$. The number of particles in the anisotropic Heisenberg chain is equal to $N=13$. Each energy point presented in this figure has been obtained by numerical iterative solutions of Eq. (7). The energy E associated with the vertical axis is measured in the units of the interparticle interaction constant $J=J_d s^2$, where J_d is a constant of the dipole-dipole interaction and s is the total spin momentum of an individual particle. The magnetic field H is measured in units of J. The real value of magnetic field is expressed from the value of H by the multiplication by factor $J/g\mu_B\mu_0 s$, where g is the Lande splitting factor and μ_B is the Bohr magneton.

$$\dot{x}_i = -\alpha\frac{\partial E}{\partial x_i} \tag{14}$$

with a sufficiently small relaxation parameter α. In our next numerical simulations we perform iterative solutions of Eqs. (7). In order to relax to the closest local minimum for $H \neq 0$ in these iterations we choose the 2^N asymptotic configurations $\mathbf{x}^*=(x_1^*,x_2^*,\ldots,x_N^*)$ as initial conditions for $H=0$. For increasing values of the external field we always use the previous configuration as the initial condition. In contrast with the first order approximation [see, Eq. (12)], with increasing field two features appear here: (1) a termination of the energy levels; and (2) a fractality of the energy spectrum. The termination of the energy level is arising at an inflection point when an appropriate minimum coalesces with a saddle point. The fractality of the energy spectrum is arising in a similar manner as was described in our previous paper,[11] see also Refs. 15–19.

The full energy spectrum for $N=13$ particles is depicted in Fig. 5. From a comparison of Figs. 4 and 5 we observe that for intermediate strength of the external field $H/J<1$ the zero order energy spectrum is an excellent approximation explaining the appearance of the splitting band structures. The energy spectrum presented in Fig. 5, the "crab," shows that there are seven branches of local minima associated with a different number of domain walls (see, also for comparison, Fig. 4). There are the following configurations: two fully polarized states; there are also states associated with two, four, and six domain walls and further other states up to 12 domain walls. As in Fig. 4 the states with different fixed numbers of domain walls N_d correspond to one of seven branches of the spectrum (see Fig. 5). Each separate energy level in the single branch corresponds to a different value of the projection of the total magnetic moment m_0. At zero magnetic field all states with the same number of domain walls and different possible values of m_0 are degenerate. At switching on of the magnetic field this degeneracy is lifted and leads to the "Crab" picture presented in Figs. 4 and 5.

Thus the energy spectrum has an amazing structure. We find termination points arising at some critical fields, where certain branches become unstable. Furthermore, there are degeneracy points at level crossings when the energy associated with a different number of domain walls coincides. Any of these termination points arise when a local minimum coalesces with a saddle point and disappears. The large variety of these termination points indicates that there is a very complicated energy landscape associated with this system. The shape of this energy landscape is also very sensitive to the magnetic field H. With changing magnetic field the position of local minima or sadddle points changes. Surprisingly at certain values of the magnetic field we have other degenerate sets of states. Figure 5 reveals that at this degeneracy point, arising at the finite value of magnetic field, the number of branches is different from the set associated with zero magnetic field. Note that this degeneracy already arises in the linearized zero order spectrum, see Fig. 4. Using Eq. (9) for the zero order spectrum, one can predict the values of the critical field when these degeneracies occur. That is a degeneracy arises at the inflection points[20–23] when

$$H = \frac{2J}{\cos(\beta)}\frac{p}{q} \tag{15}$$

with the restriction $-p<q<p$. Here p and q are given by $p=N_{d_1}-N_{d_2}$ and $q=m_{0_1}-m_{0_2}$, respectively, where N_{d_1} and N_{d_2} are specified by all possible domain numbers of two arbitrary domain configurations. The quantities m_{0_1} and m_{0_2} are specified by all possible corresponding magnetizations.

V. THE ENERGY BARRIERS AND RELAXATION TIMES

The important feature of the system is the energy barriers which are separating the local minima. Their number is very large, $\sim 2^{2N}$, as described in the previous section. Each of these barriers is associated with a saddle point of the energy landscape, presented by Eq. (5). Let us consider the lowest saddle points, which could play a role in a transition between these local minima. For sufficiently large values of $K/J \gg 1$ these saddle points can be described analytically. Its number is exactly equal to $2^{N-1}N$ distinct configurations and they are described by the "binary" vectors $\mathbf{x}^*$

$=(x_1^*,x_2^*,\ldots,x_{m-1}^*,y_m^*,x_{m-1}^*,\ldots,x_N^*)$ with $x_i^* \in \{0,\pi\}$ and $y_m^* = \pi/2$. These strings are natural solutions of the Euler-Lagrange equation (7). Accordingly, for $\frac{H}{K} \ll 1$, in zero order approximation, the energy of a barrier E_W associated with the lowest saddle points takes the simple form

$$E_W = \frac{K}{2} + H\sin\beta + \left(\sum_{i=1}^{m-1} + \sum_{i=m+1}^{N}\right)[-J\cos(x_i^*)\cos(x_{i-1}^*) - H\cos(\beta)\cos(x_i^*)] \quad (16)$$

with $x_i^*\{0,\pi\}$. Note that if we relate the first term of the sums (similarly to the previous section) to the number of domain walls N_d' in this saddle point configuration via

$$\left(\sum_{i=1}^{m-1} + \sum_{i=m+1}^{N}\right)\cos(x_i^*)\cos(x_{i-1}^*) = N - 1 - 2N_d' \quad (17)$$

and the second term of the sums to the zero order magnetization m_0' via

$$\left(\sum_{i=1}^{m-1} + \sum_{i=m+1}^{N}\right)\cos(x_i^*) = m_0' \quad (18)$$

we obtain the zero order energy of the barrier E_W associated with a saddle point of the energy landscape as a linear function of the magnetic field H

$$E_W = \frac{K}{2} + H\sin\beta - J(N - 1 - 2N_d') - m_0'\cos(\beta)H. \quad (19)$$

Note that the numbers of the domain walls N_d' and the spin number m_0' are specific for this saddle point and may be different from a configuration associated with a local minimum.

From the comparison of Eqs. (19) and (12) one may see that at zero field the energy positions of all these barriers are significantly higher (by the value $K/2$) than the positions of the local minima. That is, in other words such an energy landscape consists of many locally stable minima separated by large barriers. Moreover, such a landscape, in which the system evolves, exhibits an extremely complicated multivalley structure with a rapidly increasing number of local minima and saddle points $\sim N^4$ that also allows the appearance of structural disorder. This is precisely the situation arising in a glassy system and therefore we may conclude that this system is some kind of magnetic glass associated with the creation of domains (see also Refs. 24 and 25). Each of these minima corresponds to the state with some fixed number of domains, see Eq. (12). Even if such a number is fixed the states associated with different configurations or rearrangement of these domains will correspond to a different or the same degenerate minima. These energy levels do not differ much from each other; however, the barrier height between the corresponding minima increases with increasing values of $K/2$. Since all these configurations are locally stable and are separated from each other by large barriers we may conclude that some kind of a glassy state should arise here.[24,25]

Recent low temperature experimental studies of the field driven magnetization reversal of the MnNi chain indicate that the thermal dependence of the relaxation time followed an Arrhenius law. At high temperatures $T > K/2$ the activation energy is equal to 74 K, while with decreasing temperature a smaller activation energy of 55 K was observed. This crossover was ascribed to finite size effects.[26] According to our results the activation energy ΔE should be equal to the difference between the energy associated with the saddle point E_W and an energy associated with a local minima E_m [see, Eqs. (19) and (12)], that is $\Delta E = E_W - E_m$. There are a whole set of activation energies depending on the state in which the system is originally located. It is also clear that it is not possible to observe the magnetization reversal at very low temperatures and zero field since the barrier between any of these two states associated with different domain configurations is much too high. But the barriers can be lowered by applying magnetic field. For example, in the vicinity of the termination points of the energy spectra described in the previous section the position of the saddle point is very close to the energy minima. There the thermal fluctuations are able to nucleate a pair of the domain walls which upon propagation may eventually lead to a magnetization reversal. The stochastic nucleation process is normally studied via the relaxation time method.[10] The relaxation time can be expressed by the Arrhenius law as

$$\tau(T,H,N_d,N_d',m_0,m_0') = \tau_0 \exp[(E_W - E_m)/k_B T], \quad (20)$$

where E_W and E_m are defined by Eqs. (19) and (12), while the numbers N_d, N_d', m_0, and m_0' describe the number of the domain walls and values of total magnetic moments in the states associated with the minimum and a saddle point involved in the thermally activated transition. According to this formula one may find a very large number of the relaxation times, $\sim N^4$ associated with activation processes described by the numbers N_d, N_d', m_0, and m_0'. Note that the formula (20) has been received in the limit of the small magnetic field, i.e., $H < J \ll K$. Nonetheless, the multiplicity and the complexity of the energy landscape remain beyond this approximation. It is important to note that some of these activation processes associated with different relaxation times are more probable than the others. This is mostly related to the basin of the attraction of the state. Large broad minima of the configurational space have obviously large basins of attraction, while small shallow minima probably will be less occupied. Of course because of such complicated energy landscapes we expect that the system may display a large variety of coercive fields, or "mean nucleation fields,"[10] which can be associated with a large variety of hysteresis loops. Indeed it was found that Mn_2Ni chains display smooth hysteresis loops which are strongly temperature and field sweep rate dependent.[10]

VI. COERCIVE FIELDS AND HYSTERESIS LOOPS

Usually any magnetic system is characterized by the dependence of the total magnetization on the magnetic field when the magnetic field is varying in a large range. A closed cycle of such dependence is known as a magnetization loop. Averaged over many cycles obtained with increasing and decreasing magnetic field it is known as a hysteresis loop. Any

magnetic system is characterized by its own hysteresis loop which may be temperature and field sweep rate dependent or independent. Let us now continue to consider our linear chain and study possible hysteresis loops which could arise there. For the linear chain consisting of a finite number of magnetic particles the studies of the magnetization loops are especially important. They may provide information about the interaction between particles and give some characterisation of a glassy state arising in such systems. The hysteresis loops of course may characterize a nonequilibrium state and may reveal many additional features of our system such as the scale and variety of the barriers, their dependence on magnetic field, and others. In fact we found here that many types of magnetization loop are possible, which may give rise to many types of hysteresis loop, including a large variety of minor loops and returned branches associated with different coercive forces.[20–23] The existence of these loops is related to the complex energy landscape having very many local minima separated by large barriers. The application of a magnetic field will destabilize such configurations associated with locally stable minima in a way that the number of the minima decreases. Each of all these instabilities corresponds to a termination point of the energy spectrum or an inflection point as discussed in Sec. III (see Fig. 2). For such instability different configurations will have different critical fields. In the limit of zero magnetic field the coercive fields or the values of magnetization at zero field are described by the following analytic expression:

$$M(H=0)=\frac{m_0}{N}\cos\beta=\frac{N_+-N_-}{N}\cos\beta. \tag{21}$$

In analogy to the spectrum of the energy dependencies on external magnetic field H, depicted in Fig. 5, we now present the spectrum of magnetization dependencies on external magnetic field H, i.e., all possible total magnetizations M as a function of the external magnetic field H for fixed values of K and β. For the number of particles $N=13$ this spectrum of magnetizations is presented by discrete points in Fig. 6. The presentation in the form of points is used just for convenience since the results are obtained numerically with discrete steps in magnetic field. Each point has been obtained by numerical solutions of the Eq. (7) and then the value of M has been calculated with the aid of Eq. (6).

It is obvious from Fig. 6 that there are many branches of $m(H)$ which should be a continuous function of magnetic field. However, similar to the energy spectrum presented in Fig. 5 with increasing field there are two similar features here: (1) a termination of the magnetization branches $M(H)$ at some critical fields, H_{ci}; and (2) a fractality of the magnetization values or bifurcations of branches leading to a fractal arising at nonzero field only. The termination of magnetization branches is arising exactly at the points when a termination of the energy level is arising, that is at an inflection point when an appropriate minimum coalesces with a saddle point. The bifurcations of branches leading to a fractality of the magnetization branches is arising in a similar manner as was described in our previous paper.[11] For $N=13$ and $H=0$ we find exactly 13 distinct magnetization values described

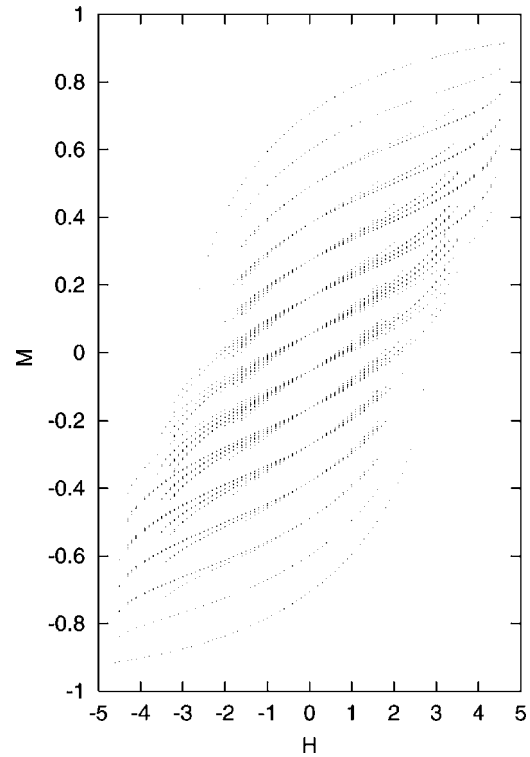

FIG. 6. Distribution or a spectrum of the total magnetizations M associated with local minima as a function of the magnetic field H for $K=5.5J$, $N=13$, and $\beta=\frac{\pi}{4}$. Each point has been obtained by numerical solutions of Eq. (7) and then the value of M has been calculated with the aid of Eq. (6). At nonzero magnetic field the magnetization set displays some features of a fractal, see, for details, Ref. 11. The magnetization M associated with a vertical axes is measured in the units of $g\mu_B\mu_0 s/N$. The magnetic field H is measured in the units of J. The real value of magnetic field may be obtained from the value of H by the multiplication of $J/g\mu_B\mu_0 s$, where g is the Lande splitting factor and μ_B is the Bohr magneton.

by Eq. (21). The highest magnetization corresponds to the homogeneous configuration with all 13 spins up $N_+=N=13$ and $N_-=0$, followed by the configurations with $12,11,10,\ldots,2,1$ and eventually all spins down, where $N_+=0$ and $N_-=13$. Note also that in contrast to the energy spectrum, where the distribution of the magnetizations has the symmetry $E(H)=E(-H)$, we have the symmetry $M(H)=-M(-H)$.

Comparable to the energy spectrum depicted in Fig. 5 the magnetization is also a multivalued function of the magnetic field H (see Fig. 6) suggesting that a variety of different hysteresis loops are theoretically possible. Indeed this suggestion is in strong agreement with recent experimental studies of Mn_2Ni.[10] However, we would like to look on this set of magnetization values from a different point of view. We are interested to determine from the magnetization dependence how transitions between the different minima may arise. In particular, the change of the magnetization m as a function of the field H may not necessarily be smooth but can increase in steps that are associated with the transitions from one minimum into another one. This fundamental mechanism giving rise to a series of minute jumps in the

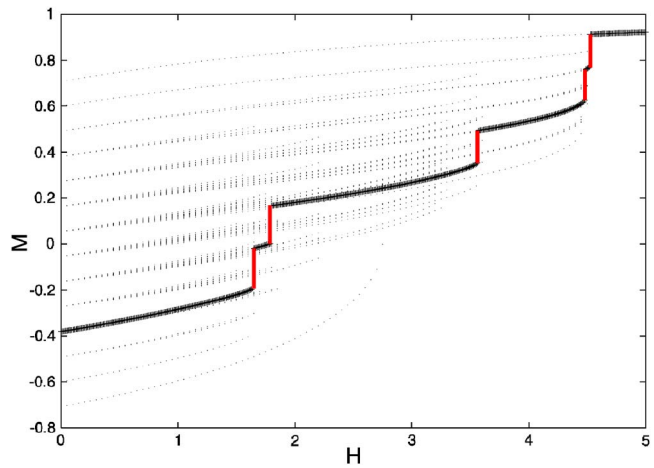

FIG. 7. (Color online) The returned branch of the magnetizations M as a function of the magnetic field H for $K=5.5J$, $N=13$, and $\beta=\frac{\pi}{4}$ presented by a bold line with discontinuous jumps. The full magnetization spectrum represented with dots serves as a guide for the eye and as an illustration of how the returned branch (the bold discotinuous line) is formed from the whole magnetization set presented in the background. Each point or dot has been obtained by numerical solutions of Eq. (7) and then the value of M has been calculated with the aid of Eq. (6). The magnetization M associated with a vertical axes is measured in the units of $g\mu_B\mu_0 s/N$. The magnetic field H is measured in the units of J. The real value of magnetic field may be obtained from the value of H by the multiplication of $J/g\mu_B\mu_0 s$, where g is the Lande splitting factor and μ_B is the Bohr magneton.

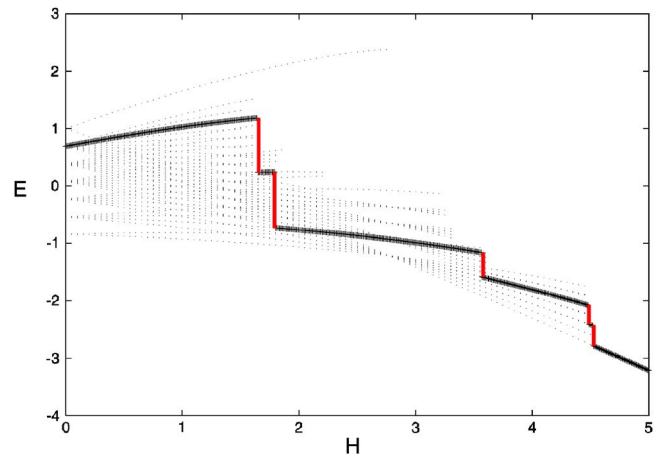

FIG. 8. (Color online) The energy E associated with a returned branch of a hysteresis loop as a function of H for $N=13$, $\beta=\frac{\pi}{4}$, and $K=5.5J$ represented by a bold discontinuous line with jumps. The full energy spectrum is represented in the background of the figure by dots and serves as a guide for the eye. Each dot has been obtained by numerical solutions of Eqs. (7). The energy E associated with a vertical axes is measured in the units of the interparticle interaction constant $J=J_d s^2$, where J_d is a constant of the dipole-dipole interaction and s is the total spin momentum of an individual particle. The magnetic field H is measured in the units of J. The real value of magnetic field is expressed from the value of H by the multiplication of the factor $J/g\mu_B\mu_0 s$, where g is the Lande splitting factor and μ_B is the Bohr magneton.

magnetization is the so-called Barkhausen effect.[21] It was discovered in 1919 and gave the first experimental evidence of these magnetic instabilities. In order to illustrate how these discontinuities in the hysteresis curve may emerge we choose an arbitrary initial configuration specified by the number of domain walls N_d and the zero order magnetization m_0 such that we are in a specific subbranch of the energy or in the corresponding magnetization $m=m_0/N\cos\beta$, respectively. Then we drive the magnetic field slowly up with a constant sweep rate. This results in a slight change of the energy landscape. With such changes of magnetic field some minima become deeper. Some other minima are getting more shallow and at some critical field disappear. Whenever such a returned branch of magnetization loses stability the system will immediately relax or jump to a still existing local minimum "nearby." Note that the nature of these jumps, and the number and the range of magnetic field between the jumps, depends on the stepsize (or sweep rate) with which the external field increases as well as on the accuracy of the calculation. The influence of thermal fluctuations existing in real experiments in the measurements of hysteresis loops might be comparable to the change of the step size in our numerical experiments. The results of such numerical experiments are depicted in Fig. 7, which illustrates how the magnetization of the chain changes on the returned branch of a hysteresis when the magnetic field increases slowly from zero. The initial value for the magnetization was taken as $m(0)=m_0/N\cos\frac{\pi}{4}=-5/13\sqrt{2}$. We observe that with increasing magnetic field the magnetization is always increasing. Moreover, we notice that with increasing field there appears five critical fields H_{ci} (see Fig. 7), where the magnetization suddenly jumps to a higher value. The corresponding energy dependence is shown in Fig. 8. It is interesting to compare Figs. 7 and 8. We may see there that the discontinuous changes in the energy are arising at the same critical fields H_{ci} as the discontinuous changes in the magnetization. We also see that during the first continuous interval of the slow increase of the magnetization that the energy also increases continuously. This means that the system remains topologically in the same local minimum which continuously changes its position. However, at the first jump in magnetization the energy jumps to a lower value. In this moment a dramatic change in the energy landscape occurs. Namely this local minimum with which this energy level was associated ceases to exist. This happens just at the inflection point and the system jumps into another nearby local minimum with a lower energy.

In a similar manner, as we can see from Figs. 7 and 8, with increasing external field H more and more domain wall configurations, corresponding to locally stable energy minima, cease to exist. The system is forced to jump into another local minimum each time when it reaches an inflection point. Depending on the degree of stability these energy minima exist even during large changes of the magneticfield. Eventually, at a very large field the system will inevitably relax to the global minimum (ground state) associated with the fully polarized configuration (see Figs. 7 and 8). Due to a highly complicated energy landscape many different series of jumps can occur. This primarily depends on the initial con-

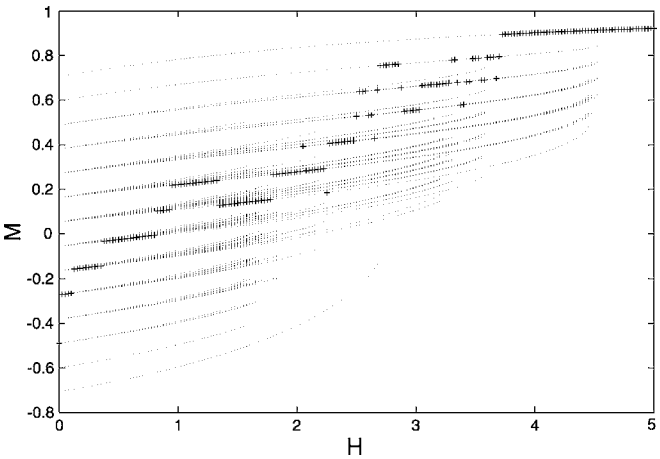

FIG. 9. The magnetic field dependence of magnetization $M(H)$ associated with a returned branch of a hysteresis loop for $K=5.5$, $N=13$, and $\beta=\frac{\pi}{4}$ and represented by a bold discontinuous line with jumps. The full magnetization spectrum is represented in the background of the figure by dots and serves as a guide for the eye. Each point dot has been obtained by numerical solutions of Eqs. (7) and then the value of M has been calculated with the aid of Eq. (6). Here we present only one returned branch from very many possible. Due to fluctuations there are transitions both with increasing and decreasing magnetization.

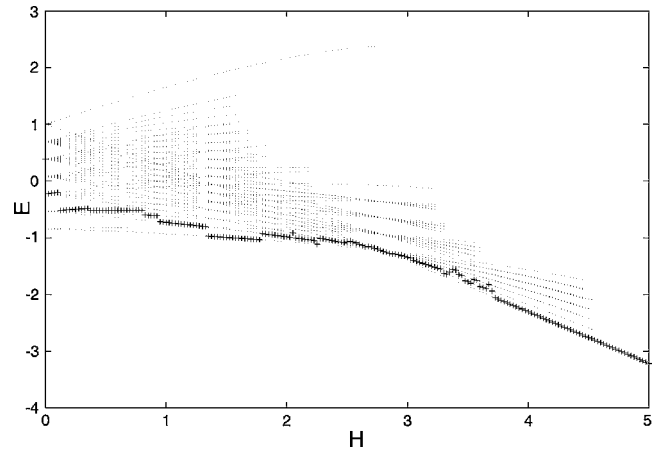

FIG. 10. The energy of local minima E as a function of H associated with a returned branch of a hysteresis loop presented in Fig. 6 represented by a bold discontinuous line for $N=13$, $\beta=\frac{\pi}{4}$, and $K=5.5J$. The full spectrum is represented with dots and serves as a guide for the eye. Each point has been obtained by numerical solutions of Eq. (7). The energy E associated with a vertical axis is measured in the units of the interparticle interaction constant $J=J_d s^2$, where J_d is a constant of the dipole-dipole interaction and s is the total spin momentum of an individual particle. The magnetic field H is measured in the units of J. The real value of magnetic field is expressed from the value of H by the multiplication of the factor $J/g\mu_B\mu_0 s$, where g is the Lande splitting factor and μ_B is the Bohr magneton.

figuration from which the system evolves. Choosing the initial condition for the magnetization randomly, one may reach many different series of jumps in the magnetization of the system. In Figs. 7 and 8, for example, we have only presented one possible series of jumps. The structure and sequence of the experimentally observed series of jumps may be different from what we have presented in Fig. 8 since it would be difficult to choose exactly the same initial conditions as we have. Nonetheless such studies may reveal many interesting characteristics of the interaction arising between magnetic particles as well as their other physical properties. Additional factors which can stimulate such Barkhausen jumps can be thermal fluctuations as well as various noises existing in the system.

In another series of our computer experiments we study the influence of noise. After each step where the field is increased we put some moderate noise into the configuration specifying the last locally stable minimum such that the initial configuration for the next value of external field is moderately disturbed. Figure 9 depicts these jumps arising at the presence of noise on a returned branch of the hysteresis curve. One may notice that with the presence of the noise the number of such jumps increases. The jumps also may lead not only to the increase of the magnetization but also to a decrease of it. Such behavior can be also found in real experimental measurements of the returned branches at finite low temperatures. The corresponding energy spectrum associated with the presented returned branch is depicted in Fig. 10.

A fluctuation associated with the noise may create its own jump which may arise not only at the inflection point. As a result the number of jumps increases, as we see, in Figs. 9 and 10. When such fluctuations are present a jump in magnetization and in the energy is definitely possible, even if the local minimum does not disappear. Such jumps can already arise when the minimum is shallow enough. Then thermal fluctuation will push the system into another local minimum. In such a series of steps it is not necessarily that the energy always decreases at each step. There may arise steps when the energy will increase and the magnetization will be decreased, see Figs. 9 and 10, respectively. Only at very large fields will the system be thermalized to the global minimum. Thus the existence of the noise and thermal fluctuations will lead to an increase in the variety of the series of Barkhausen jumps in magnetization, which we expect to be observed in future experiments. Note that when the magnetization increases continuously the system is in a specific domain structure, i.e., it is trapped in a specific local energy minimum. If thermal fluctuations are neglected and the energy barriers separating this minimum from neighboring ones are large enough, that arises here at zero field, $H=0$ and $K \gg J$, the system will indefinitely remain in such a metastable state. However, a slight change of the strength of the applied field H can decrease the barrier height and therewith destabilize a specific domain structure. For that it is sufficient that, due to the increase of the magnetic field, a local minimum of the energy landscape is transformed into a saddle point such that the system can evolve toward some other metastable configuration. These rearrangements can be quite localized in space or may involve even the whole domain structure. However, it is important to note the studies of such jumps may reveal many useful facts about the interaction, about the energy landscape, as well as about the glassy character of the behavior of the chains made of magnetic particles.

VII. SUMMARY

In the present work we have developed a theory describing a chain of monodomain magnetic particles in an external magnetic field. The theory is in excellent agreement with our numerical experiments which we have performed for five nanoparticles made from Fe deposited on a Si substrate. Our theory describes well the energy spectrum and energy landscape of the system consisting of any number of single domain magnetic particles. We have found that this energy landscape has a very peculiar structure that is associated with exponentially many minima separated by large barriers. The minima correspond to different stable domain configurations which may be useful for a construction that performs logic within a MQCA scheme.[7–9] Moreover, the described energy landscape, associated with the creation of such domains as well as fractal values of the total magnetization, may also be useful for other various applications. Because the energy surface consists of many locally stable minima that are separated by very large barriers, the chains of magnetic particles have a strong memory effect and therefore may operate as data storage. For typical chains used in the constructions of MQCA[7–9] we have estimated the heights of these barriers. So, with the use of our numerical modeling we got that the constant of the interparticle interaction is about 0.3 eV. The heights of these barriers are of the order of J_0, thus corresponding to around 3000 K. Such high values of the barriers indicate that if we store any information in the form of a particular magnetic (domain) configuration, then at room temperatures it will be preserved forever. Only the application of an external current or field can decrease the heights of these barriers and allow the change of or the clearance of the stored information. Such a property in a system of magnetic particles may be very useful for various magnetic devices. In particular this may stabilize the work of MRAM and QMCA made of chains of magnetic particles.

Each of these minima corresponds to the state with some fixed number of domains or domain walls. Even if such a number is fixed the states associated with different configurations or rearrangements of these domains will correspond to different or the same minima. This is the situation, which is precisely arising in glassy systems. Such shapes of the energy landscape led us to the conclusion that the systems formed from magnetic particles are some kind of magnetic glass. Such a glass is related to the creation and the localization of domains. We propose to make a detailed experimental investigation of these chains, made of small magnetic particles, to identify this glassy character and fractal features associated with the interaction between domains and their domain structure as well as the influence of the fractal structure on the operation of these chains. In this respect it might be useful to measure the magnetization at zero field as well as in cooled regimes as is commonly practiced in experiments on spin glasses. Due to the energy landscape described above the corresponding magnetic structure at very low temperatures are very stable with respect to thermal as well as to quantum fluctuations. To reveal these fractals experiments associated with fast cooling should be set up. The repetition of the fast cooling from high temperatures at different magnetic field strengths may drive the system to settle in the different valley of the energy landscape. The next slow increase of magnetic field may reveal a series of Barkhausen jumps displayed on returned branches of the hysteresis loops. The measuring of the total magnetization at each lap of cooling, with the same and different cooling rates, may provide the set of values of magnetization which can be reminicent of some bits of a fractal. The latter will depend on the shape and the number of particles of which the nanostructure is formed. Since the different clusters will be associated with different fractals then in general these studies may lead to the development of a new type of spectroscopy where with the aid of the fast cooling and slow field changes magnetization measurements, especially on the returned branches of the hysteresis, the structure of small clusters may be identified.[11] This is especially very convenient to do with the use of the newly developed air liquid pulse tube coolers.[27] A similar glassy structure may arise in granular high temperature superconductors where classical orbital moments are arising due to circular persistent currents flowing between the grains (see, for details, Ref. 28). This current is due to a Josephson effect and is flowing between the grains forming a Josephson network with π-junctions or a network of π-rings. The latter are arising due to the d-wave symmetry of the superconducting order parameter. Such orbital magnetic moments give rise to a paramagnetic response of the superconductor, i.e., to the paramagnetic Meissner effect[28] originally observed in Refs. 29 and 30. A chain or a planar array of electrically isolated π-rings could be treated as a set of magnetic moments oriented perpendicular to the plane (Ising spins) and interacting via magnetic dipole forces. The properties of such one-dimensional chains now attract widespread attention (see, for example, Refs. 31–33) and are very similar to the properties of the magnetic chain described in the present paper. The found phenomena of the fractal and glass formation have a very general character and may arise in many different systems, ranging from chains of spins embedded in magnetic semiconductors to the chain of magnetic particles. The described phenomena must definitely be taken into account in the design of any MQCA system made of small magnetic particles having the potential for technical applications.

ACKNOWLEDGMENTS

The authors thank D. Suess and John Samson for useful discussions. We also thank P. Martin, S. Charpentier, and M. Olivier of the Université du Littoral de Dunkerque for helpful computer assistance. The work has been supported by European Science Foundation in the framework of the network-programme: Arrays of Quantum Dots and Josephson Junctions as well as EPSRC Grant No. GR/S05052/01.

[1] *Science and Technology of Nanostructured Magnetic Materials*, edited by G. C. Hadjipanyis and G. A. Prinz (Plenum Press, New York, 1991).
[2] Y. D. Zhang, W. A. Hines, J. I. Budnick, D. P. Yang, B. G. Shen, and Z. H. Cheng, IEEE Trans. Magn. **37**, 2275 (2001).
[3] S. Asakura, S. Ishio, A. Okada, and H. Saito, J. Magn. Magn. Mater. **240**, 485 (2002).
[4] Yimei Zhu, J. W. Lau, and V. V. Volkov, Abstract of the American Physical Society meeting in Baltimore, Maryland, March 13, 2006 (unpublished).
[5] R. P. Cowburn and M. E. Welland, Science **287**, 1466 (2000).
[6] R. P. Cowburn, Phys. Rev. B **65**, 092409 (2002).
[7] D. A. Allwood, G. Xiong, C. C. Faulkner, D. Atkinson, D. Petit, and R. P. Cowburn, Science **309**, 1688 (2005).
[8] F. V. Kusmartsev and K. E. Kürten, *Spin Flop Transitions Associated Magnetic Structures and Quantum Cellular Automata*, in Condensed Matter Theories, edited by J. Clark (Nova Science, New York, 2005), Vol. 20.
[9] R. P. Cowburn, Science **311**, 183 (2006).
[10] W. Wernsdorfer, R. Clerac, C. Coulon, L. Lecren, and H. Miyasaka, Phys. Rev. Lett. **95**, 237203 (2005).
[11] K. E. Kürten and F. V. Kusmartsev, Phys. Rev. B **72**, 014433 (2005).
[12] A. Morrish, *The Physical Principles of Magnetism* (Wiley, New York, 1965).
[13] P. Vavassori, M. Grimsditch, V. Novosad, V. Metlushko, and B. Illic, Phys. Rev. B **67**, 134429 (2003).
[14] B. Rumpf, Phys. Lett. A **221**, 197 (1996).
[15] P. Bak, Phys. Today **39**, 38 (1986).
[16] P. Bak and R. Bruinsma, Phys. Rev. Lett. **49**, 249 (1982).
[17] P. Bak and J. von Boehm, Phys. Rev. B **21**, 5297 (1980).
[18] K. E. Kürten, *Multistability, Phase Transitions and Fractal Structures in Magnetic Multilayers*, in Condensed Matter Theories, edited by J. Providencia (Nova Science, New York, 2003), Vol. 18.
[19] K. E. Kürten and C. Krattenthaler, *Multistability and Fractal Properties of Hamiltonian Lattice Systems*, Condensed Matter Theories, edited by E. Suraud (Nova Science, New York, 2004), Vol. 19.
[20] G. Bertotti, *Hysteresis in Magnetism* (Academic Press, San Diego, 1998).
[21] H. Barkhausen, für Fusik **20**, 401 (1919).
[22] G. Durin, A. Magni, and G. Bertotti, J. Magn. Magn. Mater. **140-144**, 1835 (1995).
[23] G. Bertotti, B. Basso, C. Beatrice, M. Lobue, A. Magni, and P. Tiberto, J. Magn. Magn. Mater. **226-230**, 1206 (2001).
[24] D. Feinberg and F. V. Kusmartsev, *Physics in Local Lattice Distortions*, edited by A. Oyanagi and A. Bianconi (AIP, New York, 2001), p. 262.
[25] P. E. Jönsson, S. Felton, P. Svedlindh, P. Nordblad, and M. F. Hansen, Phys. Rev. B **64**, 212402 (2001).
[26] C. Coulon, Rodolphe Clérac, Lollita Lecren, Wolfgang Wernsdorfer, and Hitoshi Miyasaka, Phys. Rev. B **69**, 132408 (2004).
[27] Air liquid pulse tube coolers, http://www.dta.airliquide.com
[28] F. V. Kusmartsev, Phys. Rev. Lett. **69**, 2268 (1992).
[29] P. Svedlindh, K. Niskanen, P. Norling, P. Nordblad, L. Lundgren, B. Lönnberg, and T. Lundström, Physica C **162-164**, 1365 (1989).
[30] W. Braunisch, N. Knauf, V. Kataev, S. Neuhausen, A. Grütz, A. Kock, B. Roden, D. Khomskii, and D. Wohlleben, Phys. Rev. Lett. **68**, 1908 (1992).
[31] F. V. Kusmartsev, D. M. Forrester, M. S. Garelli, in *Physics of Superconducting Phase Shift Devices*, edited by A. Barone *et al.* (Ischia, Napoli, 2005, p. 21).
[32] H. Hilgenkamp, Ariando, H.-J. H. Smilde, D. H. A. Blank, G. Rijnders, H. Rogalla, J. R. Kirtley, and C. C. Tsuei, Nature (London) **422**, 50 (2003).
[33] J. R. Kirtley, C. C. Tsuei, Ariando, H.-J. H. Smilde, and H. Hilgenkamp, cond-mat/0503236 (to be published).